sustainability

MDPI

Article

Fracture Behavior of AlMg4.5Mn Weld Metal at Different Temperatures under Impact Loading

Radica Prokić Cvetković [1], Olivera Popović [1], Ljubica Radović [2], Aleksandar Sedmak [1,*] and Ivana Cvetković [1]

[1] Faculty of Mechanical Engineering, University of Belgrade, 11120 Kraljice Marije, 11132 Belgrade, Serbia
[2] Military-Technical Institute, Ratka Resanovica 2, 11132 Belgrade, Serbia
* Correspondence: asedmak@mas.bg.ac.rs

Abstract: This paper deals with a three-component aluminum alloy AlMg4.5Mn that was welded using a GTAW process in the shielded atmosphere of Ar+70%He+0.015%N_2. The weld-metal toughness was evaluated at three different temperatures using instrumental Charpy pendulum impact testing to measure not only the total energy, but also the crack initiation energy and the crack growth energy. Fractographic analysis of the fracture surfaces and EDS analysis of large second-phase particles on fractured surfaces at each temperature were also carried out. Fractographic analysis at different temperatures indicated a clearly distinguishable fracture mechanism. It was inferred that the absorbed energy was closely correlated with the fracturing of surfaces. Moreover, it was concluded that with decrease in the amount of microscopic voids and dimples, the total energy absorbed also decreased.

Keywords: AlMg4.5Mn alloy; GTAW; weld metal; fracture surface; fracture mechanism

Citation: Prokić Cvetković, R.; Popović, O.; Radović, L.; Sedmak, A.; Cvetković, I. Fracture Behavior of AlMg4.5Mn Weld Metal at Different Temperatures under Impact Loading. *Sustainability* **2023**, *15*, 1550. https://doi.org/10.3390/su15021550

Academic Editors: Marijana Hadzima-Nyarko and Dorin Radu

Received: 13 December 2022
Revised: 6 January 2023
Accepted: 10 January 2023
Published: 13 January 2023

1. Introduction

Aluminum and its alloys are commonly used materials for advanced applications. Due to certain existing problems, non-heat-treatable Al alloys have come to replace widely used, heat-treatable, high-strength aluminum to eliminate quenching as the cause of distortion issues [1]. Furthermore, non-heat-treatable Al alloys show good corrosion resistance and formability [2–4]. Therefore, AlMg4.5Mn alloy is widely used for liquefied gas transport, storage reservoirs and tanks, high-pressure vessels, and in the car and railway industry, as well as in shipyards. It belongs to the group of non-heat-treatable alloys whose main advantages are high strength, corrosion- and wear-resistance and good weldability [5]. In relation to its constantly increasing application in various areas, there have been numerous attempts to improve the characteristics of the AlMg4.5Mn alloy, including improvements in welding and shaping procedures [6,7]. Several problems occur in the process of aluminum alloy welding. These include the appearance of pores as the result of hydrogen absorption from the air [8], cracking—especially hot cracks occurring as the result of phase transformation in the weld metal and the heat-affected zone, as well as the chemical composition, the presence of inclusions (mostly Al_2O_3) [9], corrosion stability reduction [10–12], decrease in mechanical properties of the weld metal and the heat-affected zone [13], development of oxide films that must be dispersed, either before or during the process of welding, feeding issues with aluminum wire, and precise identification of the weld pool [14,15]. The welding process when conducted in the shielded atmosphere of mixed gases offers numerous benefits and advantages in comparison to the use of pure gases. These advantages include better liquidity, more efficient transfer of filler metals, stabilization of the electric arc, higher penetration, lower spattering and increase in welding speed [16,17]. Moreover, in the case of special gas mixtures, as used in this investigation (Ar+70%He+0.015%N_2), more heat can be generated and used for welding, which is of utmost importance for the production of alloys based on Al and Cu, since they have very large heat conductivity.

With respect to impact loading, impact toughness is the most important material property, defined by Charpy more than 120 years ago as the energy required to break a

notched specimen by a single pendulum strike. Later, by introduction of an instrumented pendulum, this energy was separated into the energy for crack initiation and for crack propagation, bringing new benefits from this simple, but effective, testing process. Understanding these energies is of utmost importance for all constructions subject to impact loading, especially welded ones, because materials with dominant crack initiation energy exhibit completely different behavior from materials with dominant crack propagation energy, even though they have the same total energy. Numerous investigations have been carried out in this field, as described briefly in the following text.

The authors of [18] reviewed the historical development of the instrumented Charpy test and discussed the load-energy time parameters that can be determined to assess material strength and fracture toughness initiation, propagation, and arrest behavior. A brief historical review of the general development of material impact testing is also provided in [19], highlighting several phases in the evolution of impact testing based on use of a pendulum.

One of the most important aspects of instrumented impact testing is its relation to fracture mechanics and, consequently, its use for structural integrity assessment. This aspect has been considered in many reports, including with respect to micro-mechanical material models applied to the evaluation of fracture toughness properties based on the results of instrumented Charpy tests [20], the evolution of the Charpy-V test from a quality control test to a materials evaluation tool for structural integrity assessment [21], and the master curve concept (MC) used to quantify variation in fracture toughness with temperature throughout the ductile-to-brittle transition region [22], as well as paper [18], which also provided an analysis of the application of the instrumented Charpy test to the assessment of structural integrity.

From the point of view of the heterogeneity of materials in welded joints, it is important to know not only the total impact energy, but also the energies for crack initiation and propagation in the base metal (BM), the weld metal (WM), and the heat-affected-zone (HAZ), to obtain better insight into the overall behavior under impact loading [23,24]. It is also important to know the stress-strain curves in all zones, the base metal (BM), the weld metal (WM), and the heat-affected-zone (HAZ) [25,26]. Although not directly related to impact testing, it is still of great importance to better understand the fracture behavior of heterogenous materials, such as welded joints.

The ductile–brittle transition is another important aspect of material behavior under impact loading, especially in the case of welded joints, due to their heterogeneity. An analysis of this transition was performed for welds by full three-dimensional transient analyses of Charpy impact specimens [27]. A further application of the instrumented Charpy pendulum includes the impact testing of polymers, based on a vibrational wave superimposed on the load-deflection curve, as described in [28].

The effects of the heterogeneity of welded joints made of high-temperature low-alloyed steel on their tensile and impact properties was investigated in [29,30], which indicated a detrimental effect of complex microstructure. Two different steels were tested, with the somewhat surprising result that HAZ resistance to crack initiation and propagation fracture was stronger than in weld metal, and was not much reduced compared to base metal.

Nevertheless, a review of the literature provided no data on AlMg4.5Mn weld metal fracture behavior at different temperatures under impact load. Therefore, here, Charpy specimens made of AlMg4.5Mn weld metal were tested using an instrumented pendulum at 20 °C, −90 °C and −196 °C, to determine its fracture behavior in terms of resistance to crack initiation and propagation at different temperatures. In addition, the crack initiation and propagation energies were analyzed in relation to fractographic testing, using a scanning electron microscope (SEM) to reveal ductile versus brittle behavior.

2. Materials and Methods

2.1. Base Metal

The aluminum alloy AlMg4.5Mn microstructure is shown in Figure 1. This structure is typical of rolled plates, with a fine Mg_2Al_3 precipitate on the grain boundary and relatively

large Mg_2Si and (Fe, Mn)Al_6 microconstituents. Table 1 presents its chemical composition, while Table 2 presents the tensile properties, taken as the minimum values from standard testing of round specimens of diameter 6 mm [5,31]. The results for the tensile properties, as presented in [5], showed very small scatter, of less than 1%.

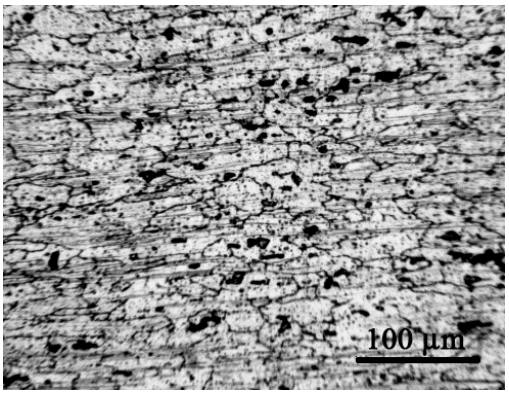

Figure 1. Aluminum alloy AlMg4.5Mn microstructure [5].

Table 1. AlMg4.5Mn chemical composition (vol. %) [5].

Si	Fe	Cu	Mn	Mg	Zn	Cr	Ti
0.13	0.21	0.04	0.66	3.95	0.03	0.06	0.025

Table 2. Aluminum alloy AlMg4.5Mn mechanical properties [5].

Direction	Tensile Strength, R_m (MPa)	Yield Stress, $R_{0.2}$ (MPa)	Elongation A (%)
Rolling	293	131	23.7
Transverse	304.4	145	25.7

2.2. Welding Procedure and Welded Joints

Testing plates made of aluminum alloy AlMg4.5Mn, sized 500 × 250 × 12 mm, with "V" grooves made by milling, were used in this research. The gas tungsten arc-welding (GTAW) process was used for the welding of testing plates with an aluminum alloy wire AlMg4.5Mn, diameter 5 mm, used as the filler material. The chemical compositions of the base metal and filler material are shown in Table 3 [31].

Table 3. Chemical composition of base metal AlMg4.5Mn and filler material, wt.%.

Element (wt.%)	Si	Fe	Cu	Mn	Mg	Zn	Cr	Ti
Base metal	0.13	0.21	0.04	0.66	3.95	0.03	0.06	0.025
Filler material	<0.40	<0.40	<0.10	0.5–1.0	4.3–5.2	<0.25	0.05–0.25	0.15

For the protection of the welded joint during GTAW process, a shielding atmosphere was used, made of a mixture of inert gases Ar+70%He+0.015%N_2. The testing plates were welded in four passes, including one root pass and four filler passes (Figure 2). The welding parameters, including current capacity, voltage, welding speed and the calculated welding heat input, are shown in Table 4.

Table 4. Welding parameters.

Current (A)	Voltage (V)	Welding Speed (cm/min)	Heat Input (kJ/cm)
192–198	20–21	15–17	13–17

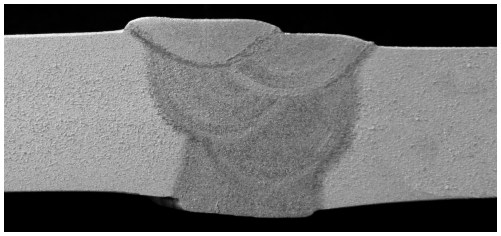

Figure 2. Macrograph of GTAW welded joint.

The ambient temperature during the process of welding was 20 °C and the preheating temperature of the plates was above 110 °C to prevent cracking during welding.

The welded joint, as a whole, was tested using standard procedure, EN895, using specimens with a rectangular cross-section, Figure 3 [31].

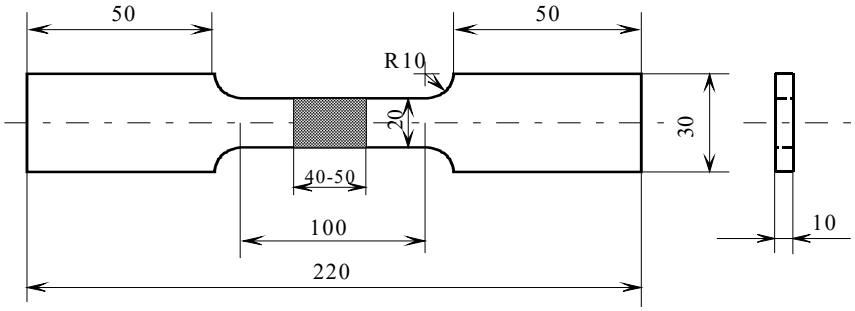

Figure 3. Specimen for tensile testing of welded joint [32].

The minimum values for tensile strength and elongations were R_m = 303.7 MPa and A = 19%, respectively, with the break-point at the fusion line [31].

2.3. Specimen Preparation for CHARPY Testing

Specimens for standard Charpy testing with a "V" notch (Figure 4a), were cut out from welded plates, with the notch located in the center of the weld metal (Figure 4b). After impact testing, fractographic analysis of the fractured surfaces was carried out.

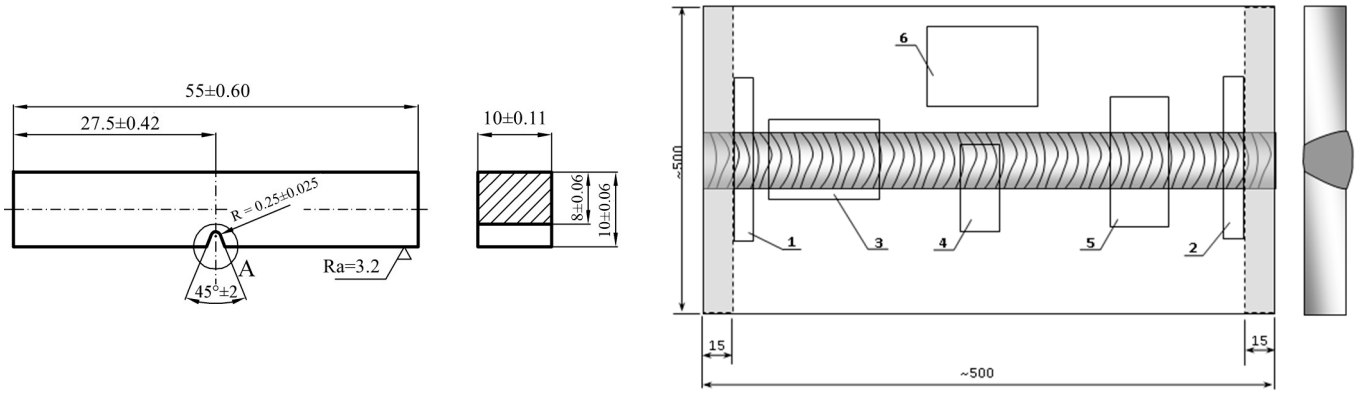

Figure 4. (**a**) Charpy specimen. (**b**) Scheme of specimen preparation: 1. metallography; 2. hardness; 3. Charpy for weld metal; 4 and 5. tensile testing; 6. Charpy for base metal.

2.4. Impact Testing on Instrumented Charpy Pendulum

Impact testing on standard Charpy specimens was performed on the instrumented Charpy pendulum, which enables separation of the total impact energy, E_t, into the crack initiation energy, E_{in}, and the crack propagation energy, E_{pr}. In Figure 5, a diagram of force

(F) versus time (t), obtained by the instrumented Charpy pendulum is shown schematically for surfaces A_i and A_p, left and right from the maximum force [31]. The ratios of A_i and A_p with the total surface are measures of the energy for crack initiation, E_i, and propagation, E_p, respectively. These two energies are recorded on the instrumented Charpy pendulum and are provided directly as the result of impact testing.

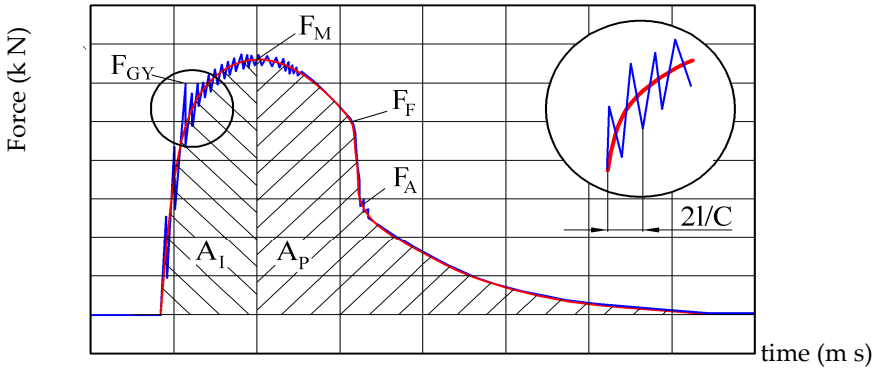

Figure 5. Separation of crack initiation and propagation energies using F–t diagram [31].

Diagrams of force (F) against time (t), obtained by use of an instrumented Charpy pendulum, are shown schematically in Figure 6, indicating different behavior relating to the crack initiation and crack propagation energies [32]. The strong effect of these two different distributions should be noted. In the case of dominant crack propagation energy, the material has high crack resistance regardless of eventual crack presence, which is not uncommon for weld metals, even if they have passed quality control by non-destructive testing (NDT). In contrast, dominant crack initiation energy is not a favorable option for weld metals.

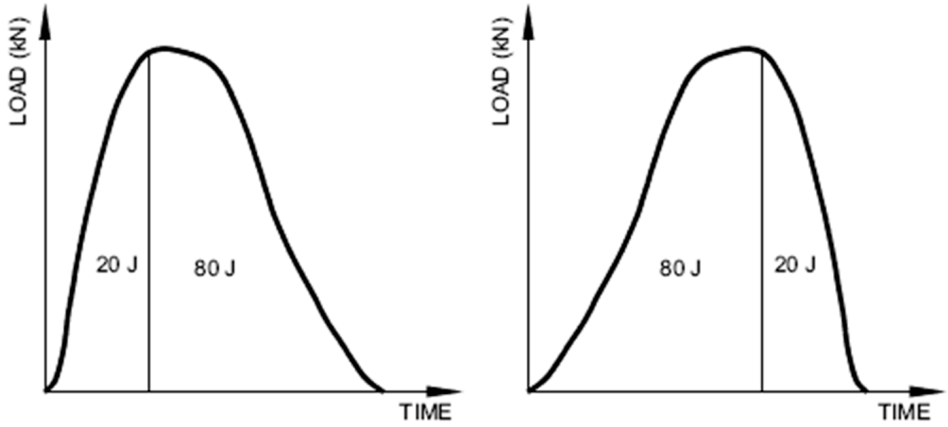

Figure 6. Schematic presentation of two opposite material behaviors with the same total energy: dominant crack propagation energy (**left**), dominant crack initiation energy, (**right**) [32].

The effect of temperature on the impact energies is shown in Figure 7, indicating that the total energy and the crack propagation energy show so-called nil-ductility temperature (a sudden drop in energy), whereas the crack initiation energy shows more gradual decrease with decreasing temperature. This represents two major issues in the analysis of weld metal impact fracture behavior: the temperature effect and the ratio between the crack initiation and the propagation energies, the latter potentially changing with decreasing temperature, as shown in Figure 7.

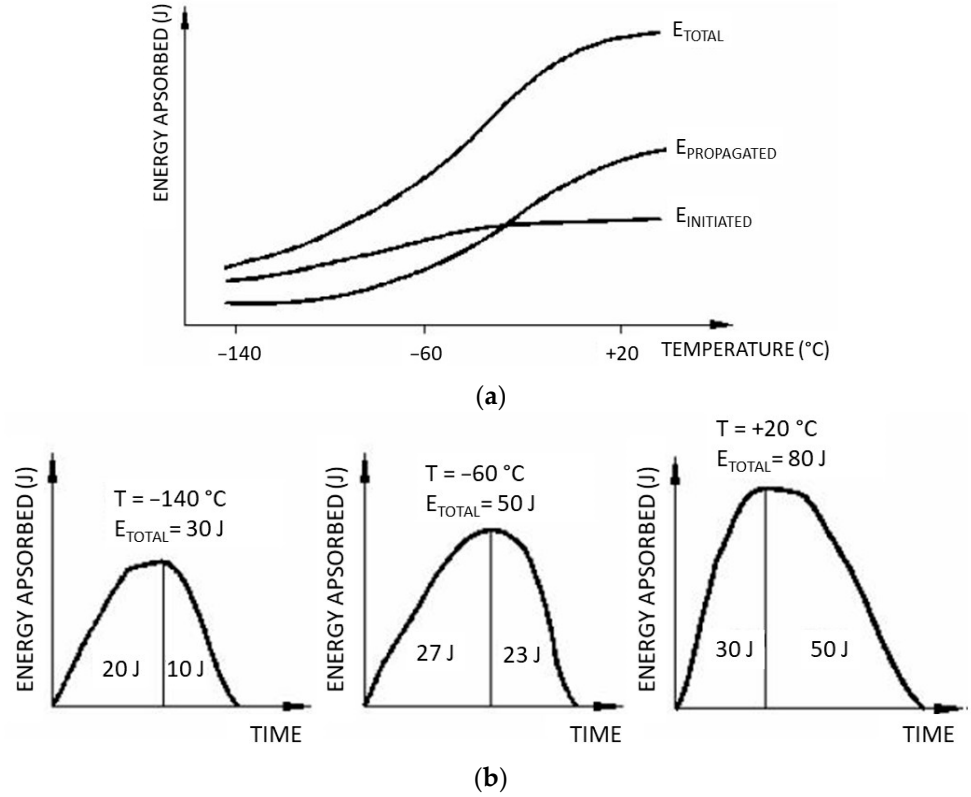

Figure 7. Schematic presentation of two opposite material behaviors with the same total energy: (**a**) dominant crack propagation energy, (**b**) dominant crack initiation energy [32].

2.5. Fractographic Examination

The fractured surfaces of the Charpy specimens were examined using a scanning electron microscope (SEM) Jeol JSM-6610 LV, with an acceleration voltage of 20 kV. This is standard equipment used in the fractographic examination of welded joints and its constituents, BM, WM and HAZ.

3. Results and Discussion

3.1. Impact Testing

A weld metal impact test on standard Charpy specimens was performed on the instrumented Charpy pendulum at temperatures 20 °C, −90 °C and −196 °C. Diagrams of force (F) versus time (t), obtained by use of an instrumented Charpy pendulum for different testing temperatures, are shown in Figure 8. The results obtained for all impact energies are shown in Figure 9 in the form of diagrams of energy versus temperature for the total energy, and the crack initiation and propagation energies. The F-t diagrams, obtained using the instrumented Charpy pendulum, indicate the type of fracture. As can be seen in Figure 8, the shape of the force–time diagrams for temperatures of 20 °C and −90 °C indicate a more ductile type of fracture, whereas the shape of the force–time diagram at −196 °C indicates a more brittle type of fracture.

The results for the total energy, as well as for the energies for crack initiation and propagation, as obtained directly from the instrumented pendulum, are presented in Table 5 for the purpose of comparison with results for the base metal obtained in [31] at 20 °C and −196 °C, as shown in Table 6. The energy values at room temperature indicate that the weld metal had slightly higher E_t, with a different distribution of E_p and E_i, the first higher and the latter lower than for the base metal, whereas all the weld metal energies were significantly lower than the corresponding base metal energies at −196 °C. The uniformity of the results, especially in the case of the base metal, is noteworthy.

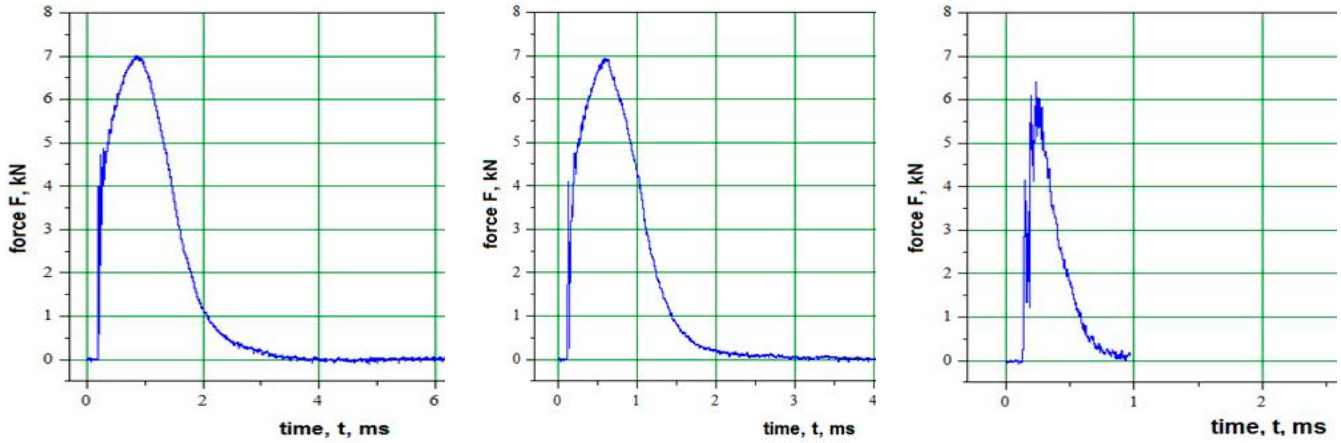

Figure 8. Diagrams F-t at different temperatures (**a**) 20 °C, (**b**) −90 °C, (**c**) −196 °C.

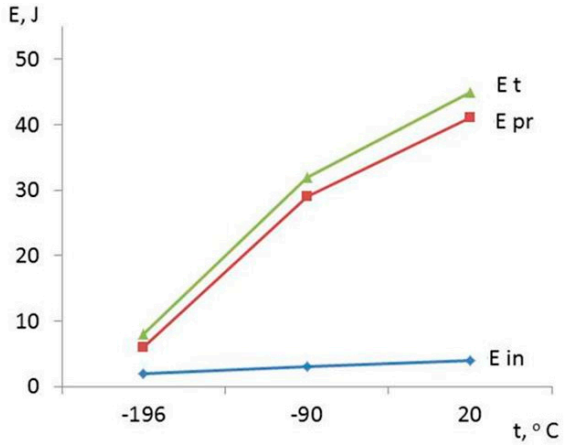

Figure 9. Impact energies vs. temperature.

Table 5. Weld metal total energy, E_t, energy for crack initiation, E_i, and propagation, E_p.

Spec. No.	20 °C			−90 °C			−196 °C		
	E_t, J	E_i, J	E_p, J	E_t, J	E_i, J	E_p, J	E_t, J	E_i, J	E_p, J
1	48	4	44	34	3	31	8.5	2	6.5
2	42	3.5	38.5	29.5	3	26.5	6.5	2	4
3	45	4	41	31	3.5	27.5	7.5	2	5.5
average	45 ± 3		41 ± 3	31 ± 3		28.5 ± 2.5	7.5 ± 1		5.5 ± 1.5

Table 6. Base metal total energy, E_t, energy for crack initiation, E_i, and propagation, E_p [31].

Direction	Spec. No.	20 °C			−196 °C		
		E_t, J	E_i, J	E_p, J	E_t, J	E_i, J	E_p, J
Rolling	1	41	12	29	28,5	11	17,5
	2	41	12	29	28	11	17
	3	40	12	28	28	11	17
Transverse	1	32	11	21	23	11	12
	2	32	11	21	22	11	11
	3	32	11	21	22	11	11

High-strength aluminum alloys are characterized by a ductile fracture mechanism, but with relatively low toughness, which means that fractures are to a greater or lesser extent brittle with respect to the level of energy and, at the same time, to a greater or lesser extent ductile with respect to the fracture mechanism. This phenomenon is also known as quasi-brittle fracture [33], but has not so far been investigated for AlMg4.5Mn weld metal. The results for the impact energies at 20 °C and −90 °C indicate similar behavior of the weld and base metals. However, there was a significant reduction in all the weld metal impact energies at −196 °C, both in absolute terms, and relative to the base metal (7.5 J vs. 22/28 J, Tables 5 and 6). At the same time, a rapid drop in force value after the maximum force F–t diagram is reached is evident (Figure 8c). These differences reflect the effect of welding on the toughness. The same data for the total impact energy for a base metal at −196 C (22 J) are also provided in [34].

Another aspect of the testing of the V-notch weld metal specimens is the ratio of the crack initiation energy, E_{in}, and the crack propagation energy, E_{pr}, which depends on the testing temperature. The total impact energy at room temperature was 45 J, while the crack growth energy was 41 J. With decrease in temperature to −90 °C, the total impact energy and crack growth energy were decreased by approximately 30%, whereas at −196 °C, they were just 15% of the room temperature value. With respect to the crack initiation energy, this was very low at all temperatures, from just 4 J at room temperature, to just 2 J at −196 °C. However, this is not of great importance for a weld metal, as already discussed, since crack-like defects in welded joints are inevitable, and, thus, the crack initiation energy should not be relied on.

It is important to emphasize that, even though the crack propagation energy was higher than the crack initiation energy, which is recommended for reliable welded structures, both energies obtained for the weld metal at −196 °C were too low, indicating a major difference in impact fracture behavior compared to the base metal.

3.2. Fractographic Testing

Fractographic testing of the specimens at different temperatures showed clearly distinguishable fracture mechanisms. Figure 10 shows the SEM fractographs of specimens tested after impact load at 20 °C. The entire fracture surface of this specimen was rough, covered with equiaxed dimples, which were quite uniform in size. At higher enlargement (Figure 7b), the particles of the secondary phases are observed on the bottom of dimples. This indicates the existence of a trans-granular fracture mechanism by void initiation, growth and coalescence. It appears that the voids are initiated mostly at constituent particles, while the coalescence occurs by impingement [35].

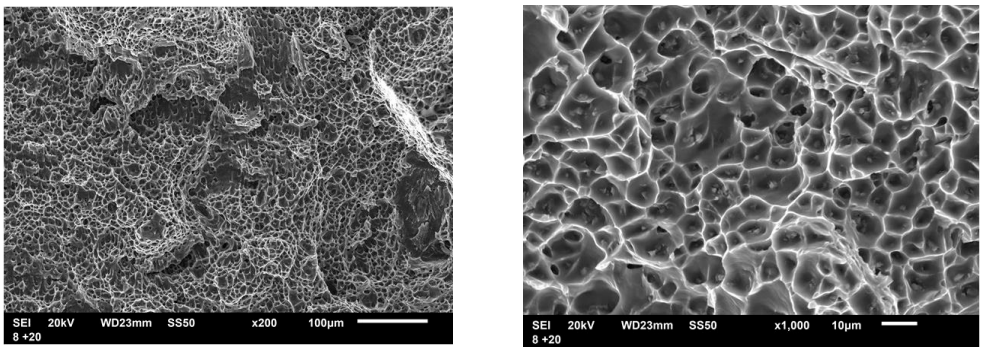

(**a**) (**b**)

Figure 10. SEM fracture surface morphology of AA5083 alloy, under impact loading at +20 °C: (**a**) ×200 magnification, (**b**) ×1000 magnification.

After the impact testing conducted at −90 °C, a dimpled fracture dominated on the fracture surface, with some smooth, wavy areas of intergranular fracture (Figure 11a). Nevertheless, when magnified, isolated dimples and numerous secondary phase particles

can be seen on this intergranular fracture surface (Figure 11b). The coalescence of dimples occurred by shearing of the inter-void ligaments and, therefore, the resulting fracture surface was smooth (Figure 11c).

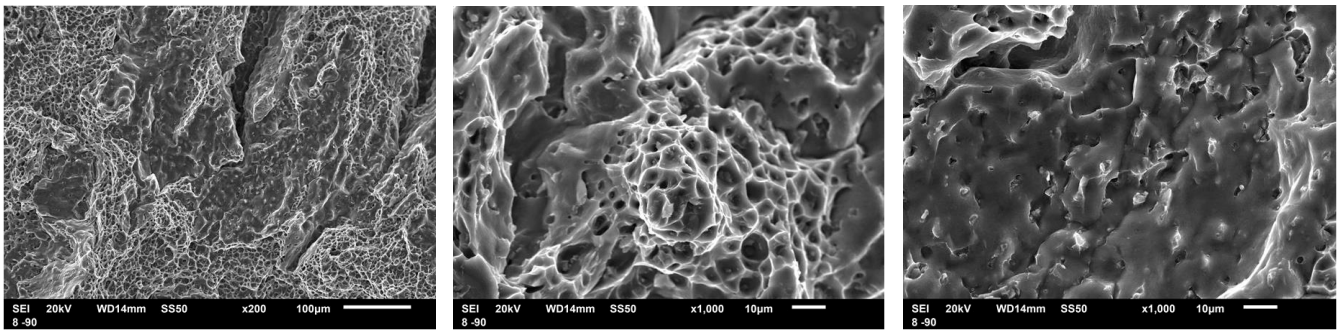

(**a**) (**b**) (**c**)

Figure 11. SEM fracture surface morphology of AA5083 alloy, under impact loading at −90 °C: (**a**) ×200 magnification; (**b**) ×1000 magnification, dimpled area; (**c**) ×1000 magnification, smooth area.

The specimen tested at −196 °C fractured in a similar manner to the specimen tested at −90 °C. However, most of the area was smooth and a very small part was dimpled (Figure 12a). Secondary cracks were observed. This type of fracture surface is usually considered an intergranular fracture [36], with isolated dimples and secondary phase particles seen on the intergranular fracture surface (Figure 12b). The intergranular fracture showed some ductility in the form of dimpled facets. It should be noted that the dimple size decreased with decrease in the testing temperature.

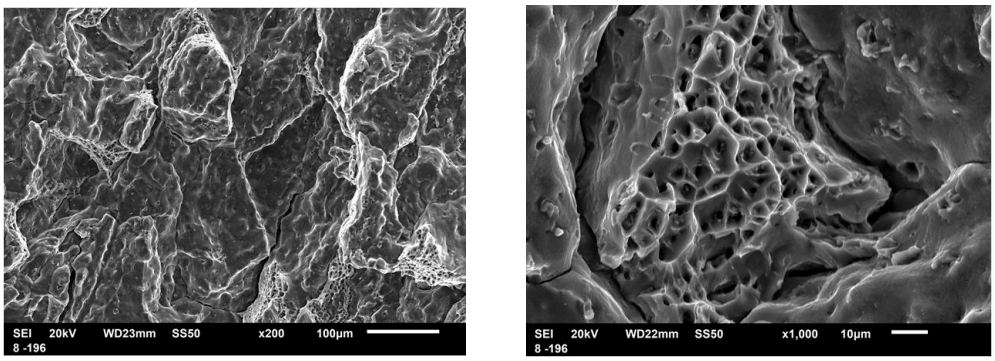

(**a**) (**b**)

Figure 12. SEM fracture surface morphology of AA5083 alloy, under impact loading at −196 °C: (**a**) ×200 magnification, (**b**) ×1000 magnification.

Voids were initiated at matrix/particle interfaces as a result of particle fracture. Fragmentations of the large second phase particles were observed at fractured surfaces at all temperatures (Figure 13). The EDS analysis revealed that these particles were present in the (Fe, Mn)Al_6 phase (Figure 14). It was previously reported that these particles are very hard and brittle [37].

A decrease in temperature led to a decrease in the dimpled fracture fraction, and caused ductile intergranular fracture, which is a characteristic feature of an FCC crystal structure [38]. Fracture at −196 °C still showed some ductility. Voids were also initiated in a similar manner as at +20 °C, but they did not grow. Low plastic deformation was caused because the active slip systems were limited at low temperatures. An increase in temperature facilitated the activation of more slip systems, resulting in high plastic deformation and, thereby, the impact energy increased. While high energy was absorbed by micro-void coalescence by impingement during ductile fracture at +20 °C, coalescence

of the voids by shearing (−90 °C and −196 °C) absorbed much less energy. At −90 °C, the crack propagation energy fell to 70% of the crack propagation energy at 20 °C, while at −196 °C, this energy fell to 15%. Therefore, the absorbed energy was closely correlated with fracturing of the surfaces. Moreover, as the quantity of microscopic voids and dimples on the fracture surfaces decreased, the total energy absorbed to fracture decreased.

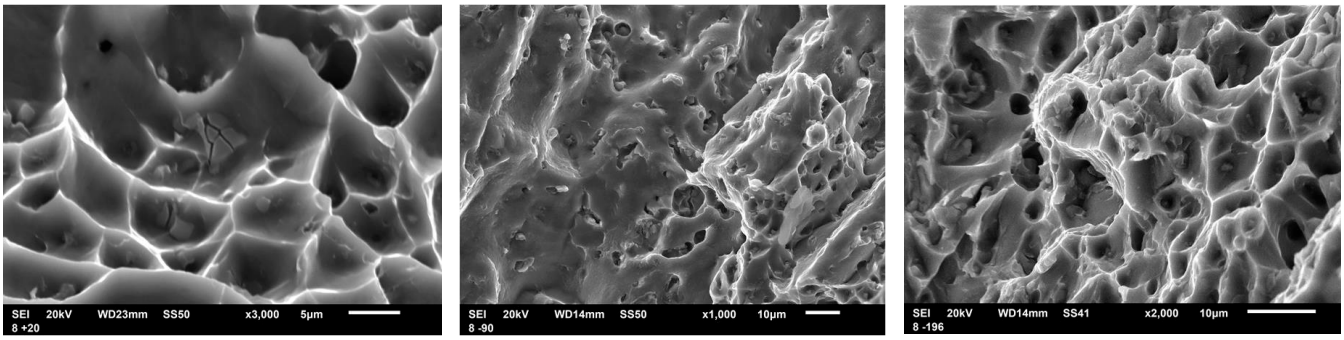

(**a**) (**b**) (**c**)

Figure 13. SEM fracture of the second phase particles after impact testing carried out at different temperatures: (**a**) 20 °C; (**b**)−90 °C; (**c**) −196 °C.

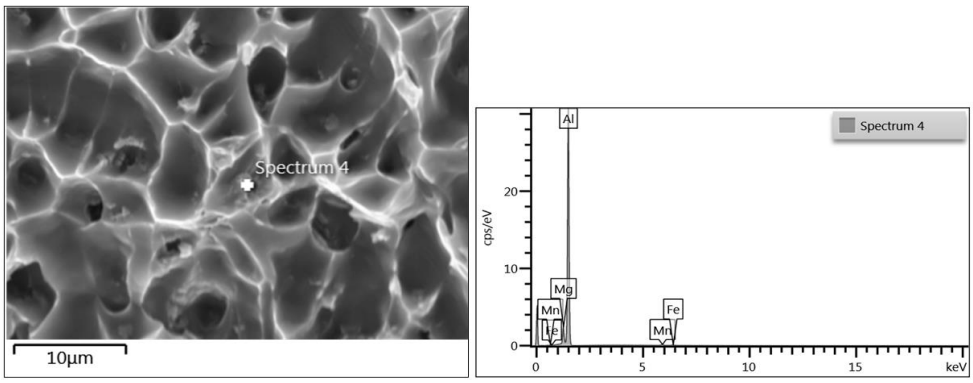

Figure 14. EDS of the second phase particles and corresponding spectrum.

4. Conclusions

Based on the presented experimental results and their analysis, the following can be concluded:

- A ductile fracture mechanism is characteristic for high strength aluminum alloys, but their toughness is relatively low. In the case of a weld metal made by GTAW, the shape of a force vs. time graph did not change with decrease in temperature from 20 °C to −90 °C, with a ductile fracture mechanism dominating at the corresponding fracture surface. However, at −196 °C, the force rapidly dropped after a maximum value, indicating dominant brittle fracture, as also seen on the fracture surface. This was obviously the effect of welding.
- Fractographic investigation of the specimens at different temperatures indicated the existence of a clearly distinguishable fracture mechanism. At room temperature, a trans-granular failure mechanism by void initiation, growth and coalescence was present. With temperature decrease, dimpled fractures dominated, but some areas of intergranular fracture were observed with a dimpled and smooth area. At a temperature of −196 °C, a significantly smaller part of the fracture surface was dimpled and intergranular ductile failure dominated.
- While high energy was absorbed by micro-void impingement coalescence during ductile fracture at +20 °C, coalescence of the voids by shearing (−90 °C and −196 °C) absorbed less energy. At −90 °C, the crack propagation energy fell to 70%, compared

to 20 °C, while, at −196 °C, this energy fell to 15%. Therefore, the absorbed energy was closely correlated with the fractured surfaces.

- As the amount and size of microscopic voids and dimples on the fracture surfaces decreased, the total energy absorbed by the fracture decreased. Decrease in temperature led to decrease in the dimpled fracture fraction. EDS analysis revealed the presence of a large second phase, with hard and brittle particles (Fe, Mn)Al_6 at the fractured surfaces at all temperatures.
- If 30 J is taken as a criterion for acceptance regarding impact energy, then −90 °C appears to be the lowest acceptable temperature for AlMg4.5Mn weld metal, whereas the base metal has a significantly lower transition temperature, close to −196 °C.

Author Contributions: Conceptualization, R.P.C. and O.P.; methodology, A.S. and R.P.C.; fractography, L.R.; writing—review and editing, O.P. and I.C.; supervision, A.S. and I.C. All authors have read and agreed to the published version of the manuscript.

Funding: This research was supported by the Ministry of Education, Science, and Technological Development of the Republic of Serbia (Contracts No. 451-03-68/2022-14/200135, 451-03-68/2022-14/200105).

Acknowledgments: This research was supported by the Ministry of Education, Science, and Technological Development of the Republic of Serbia (Contracts No. 451-03-68/2022-14/200135, 451-03-68/2022-14/200105).

Conflicts of Interest: The authors declare no conflict of interest.

Glossary

E_t	total impact energy
E_i	crack initiation energy
E_p	crack propagation energy
R_m	tensile strength
$R_{0.2}$	yield stress
A	elongation
F	force
T	time
GTAW	gas tungsten arc welding
SEM	scanning electron microscopy
EDS	energy dispersive spectroscopy

References

1. ASM. *ASM Handbook: Heat Treating*, 10th ed.; ASM International: Almere, The Netherlands, 1991; Volume 4.
2. Burger, G.B.; Gupta, A.K.; Jeffrey, P.W.; Lloyd, D.J. Microstructural control of aluminum sheet used in automotive applications. *Mater. Charact.* **1995**, *35*, 23–29. [CrossRef]
3. Horvath, G.; Chinh, N.Q.; Gubicza, J.; Lendvai, J. Plastic instabilities and dislocation densities during plastic deformation in Al-Mg alloys. *Mater. Sci. Eng. A* **2007**, *445–446*, 186–192. [CrossRef]
4. Lloyd, D.J. The deformation of commercial aluminum-magnesium alloys. *Metall. Trans. A* **1980**, *11*, 1287–1294. [CrossRef]
5. Jovičić, R.; Sedmak, A.; Prokić-Cvetković, R.; Bulatović, S.; Buyukyildirim, G. Cracking Resistance of AlMg4.5Mn Alloy TIG Welded Joints. *Struct. Integr. Life* **2011**, *11*, 205–208.
6. Jang, K.C.; Lee, D.G.; Kuk, J.M.; Kim, S.I. Welding and environmental test condition effect in weldability and strength of Al alloy. *J. Mater. Process. Technol.* **2005**, *164–165*, 1038–1045. [CrossRef]
7. Kim, J.H.; Park, D.H. Welding and characterization of 5083 aluminum alloy. *J. Korean Weld. Soc.* **1994**, *12*, 7–15.
8. Prokic-Cvetkovic, R.; Popovic, O.; Burzic, M.; Jovicic, R.; Kastelec-Macura, S.; Buyukyildirim, G. The effect of welding process and shielding atmosphere on the AlMg4.5Mn weld metal properties. *Int. J. Mater. Res.* **2013**, *104*, 18–25. [CrossRef]
9. Kastelec-Macura, S.; Prokić-Cvetković, R.; Jovičić, R.; Popović, O.; Burzić, M. Porosity of welded joints of AlMg4.5Mn alloy. *Struct. Integr. Life* **2008**, *8*, 114–120.
10. Katsas, S.; Nikolaou, J.; Papadimitriou, G. Corrosion resistance of repair welded naval aluminum alloy 5083. *Mater. Des.* **2007**, *28*, 831–836. [CrossRef]
11. Pickens, J.R.; Gordon, J.R.; Green, J. The effect of loading mode on the stress corrosion cracking of aluminum alloy 5083. *Metall. Trans.* **1983**, *14*, 925–930. [CrossRef]

12. Baer, D.R.; Windisch, C.F. Influence of Mg on the corrosion of Al. *Vac. Sci. Technol.* **2000**, *18*, 131–136. [CrossRef]
13. Burzic, Z. Modern methods for the confirmation of mechanical-technological properties of welded joints, Part 2. *Weld. Welded Struct.* **2002**, *47*, 151–158.
14. Praveen, P.; Yarlagadda, P. Meeting challenges in welding of aluminium alloys through pulse gas metal arc welding. *Mater. Process. Technol.* **2005**, *164–165*, 1106–1112. [CrossRef]
15. Atkins, G.; Thiessen, D.; Nissley, N.; Adonyi, Y. Welding Process Effects in Weldability Testing of Steels. *Weld. J.* **2002**, *4*, 61s–68s.
16. Webster, P.J.; Hughes, D.J.; Mills, G. Measurements and modelling of residual stresses in a TIG weld. *Mater. Sci. Process.* **2002**, *74*, 1421.
17. Quinn, T.P. Process Sensitivity of GMAW: Aluminum vs. Steel. *Weld. J.* **2007**, *81*, 55s–60s.
18. Server, W.L. Instrumented Charpy test review and application to structural integrity. *Eur. Struct. Integr. Soc.* **2002**, *30*, 205–212.
19. Tóth, L.; Rossmanith, H.-P.; Siewert, T.A. Historical background and development of the Charpy test. *Eur. Struct. Integr. Soc.* **2002**, *30*, 3–19.
20. Schmitt, W.; Varfolomeyev, I.; Böhme, W. Modelling of the Charpy test as a basis for toughness evaluation. *Eur. Struct. Integr. Soc.* **2002**, *30*, 45–56.
21. Wallin, K.; Nevasmaa, P.; Planman, T.; Valo, M. Evolution of the Charpy-V test from a quality control test to a materials evaluation tool for structural integrity assessment. *Eur. Struct. Integr. Soc.* **2002**, *30*, 57–68.
22. Viehrig, H.-W.; Boehmert, J.; Dzuga, J. Use of instrumented Charpy impact tests for the determination of fracture toughness values. *Eur. Struct. Integr. Soc.* **2002**, *30*, 245–252.
23. Jovanovic, M.; Camagic, I.; Sedmak, S.; Zivkovic, P.; Sedmak, A. Crack initiation and propagation resistance of HSLA steel welded joint constituents. *Struct. Integr. Life* **2020**, *20*, 11–14.
24. Jovanovic, M.; Camagic, I.; Sedmak, S.; Sedmak, A.; Burzic, Z. The Effect of Material Heterogeneity and Temperature on Impact Toughness and Fracture Resistance of SA-387 Gr. 91 Welded Joints. *Materials* **2022**, *15*, 1854. [CrossRef] [PubMed]
25. Milosevic, N.; Sedmak, A.; Bakic, G.; Lazic, V.; Milosevic, M.; Mladenovic, G.; Maslarevic, A. Determination of the actual stress–strain diagram for undermatching welded joint using DIC and FEM. *Materials* **2021**, *14*, 4691. [CrossRef]
26. Milosevic, N.; Younise, B.; Sedmak, A.; Travica, M.; Mitrovic, A. Evaluation of true stress–strain diagrams for welded joints by application of Digital Image Correlation. *Eng. Fail. Anal.* **2021**, *128*, 105609. [CrossRef]
27. Tvergaard, V.; Needleman, A. 3D Charpy specimen analyses for welds. *Eur. Struct. Integr. Soc.* **2002**, *30*, 437–444.
28. Morita, S.; Hosoi, K.; Kobayashi, T. Instrumented impact testing of polymers. *Eur. Struct. Integr. Soc.* **2002**, *30*, 155–162.
29. Jovanovic, M.; Camagic, I.; Sedmak, A.; Burzic, Z.; Sedmak, S.; Zivkovic, P. Analysis of SA 387 Gr. 91 welded joints crack resistance under static and impact load. *Procedia Struct. Integr.* **2021**, *31*, 38–44. [CrossRef]
30. Camagic, I.; Sedmak, A.; Sedmak, S.; Burzic, Z. Relation between impact and fracture toughness of A-387 Gr. B welded joint. *Procedia Struct. Integr.* **2019**, *18*, 903–907. [CrossRef]
31. Sandra, K.-M. Research of the Effects of the Welding Parameters on the Structure and Weld Properties of the AlMg4.5Mn Alloy (in Serbian). Doctoral Thesis, University of Belgrade, Belgrade, Serbia, 2011.
32. Vencislav, G.; Zijah, B.; Dejan, M. *Significance of Mechanical Testing for Structural Integrity, Monography "The Challenge of Materials and Weldments"*; IFMASS 9; MF, DIVK, TMF and GOŠA: Belgrade, Serbia, 2008; pp. 121–129.
33. ASM. Properties and Selection: Irons, Steels, and High-Performance Alloys. In *ASM Metals Handbook*, 10th ed.; ASM Materials Park: Novelty, OH, USA, 1990; Volume 1.
34. Huang, C.; Wu, Z.; Huang, R.; Wang, W.; Li, L. Mechanical properties of AA5083 in different tempers at low temperatures. *IOP Conf. Ser. Mater. Sci. Eng.* **2017**, *279*, 012002. [CrossRef]
35. Chena, Z.; Worswick, M.J. Investigation of void nucleation in Al—Mg sheet. *Mater. Sci. Eng. A* **2008**, *483–484*, 99–101. [CrossRef]
36. ASM. Fractography. In *ASM Metals Handbook*, 9th ed.; ASM Metals Park: Materials Park, OH, USA, 1987; Volume 12.
37. Radović, L.; Nikačević, M.; Jordović, B. Deformation behavior and microstructure evolution of AlMg6Mn alloy during shear spinning. *Trans. Nonferrous Met. Soc. China* **2012**, *22*, 991–1000. [CrossRef]
38. Hurlish, A. *Low Temperature Metals, Reprinted with Permission of Chemical Engineering*; McGraw-Hill Publishing Go., Inc.: New York, NY, USA, 1963.